Study on Stability of Tunnel Portal Section Based on Strength Reduction Shortest Path Method

Wei Wang, Guiqiang Gao(✉), Mingjun Hu, Yanfei Zhang, and Haojie Tao

School of Civil Engineering, Central South University, Changsha 410075, China
albertgao@csu.edu.cn

Abstract. It is very significant to maintain the stability of surrounding rock during the entire lifetime of the tunnel. Generally speaking, the stability of the surrounding rock in the portal section of the tunnel is the worst. Therefore, it is meaningful to study the instability mechanism and factors affecting the instability of the surrounding rock in the tunnel portal section. In this paper, we studied the stability of tunnel surrounding rock based on a novel double strength reduction method (the strength reduction shortest path method). The double strength reduction method was used to reduce the cohesion and internal friction angle with different reduction factors in the stability analysis of surrounding rock. We used the overall safety factor to evaluate the stability of the tunnel. The smaller the overall safety factor, the more likely the tunnel is to lose stability. The influence of strength parameters of surrounding rock on the stability of the portal section was discussed emphatically. The results show that: As the reduction ratio λ increases, the length of the strength reduction path first decreases and then increases, which indicates that there is a shortest strength reduction path; It is reasonable to take the drastic change of the vault displacement as the instability criterion; As the initial internal friction angle and the initial cohesion increase, the length of the strength reduction shortest path and the overall safety factor increase, in which the effect of the internal friction angle is more significant.

This paper can provide a new method for studying the stability of the tunnel portal section and provide a useful reference for future tunnel construction.

Keywords: Shallow buried mountain tunnel · Tunnel portal section · Surrounding rock stability · Double strength reduction method · The shortest strength reduction path method

1 Introduction

The surrounding rock of the tunnel portal section is usually severely weathered. The rock mass there is loose and broken, which probably leads to slope instability. Therefore, it is of great practical significance to analyze the instability mechanism, and factors affecting the instability of the surrounding rock in the tunnel portal section. At present, the commonly used methods for stability analysis of rock and soil mass include the limit

S. Shu et al. (Eds.): GeoChina 2021, SUCI, pp. 71–91, 2021.
https://doi.org/10.1007/978-3-030-80142-7_6

equilibrium method [1, 2], limit analysis method [3, 4], and strength reduction method [5]. Among all the methods, when using the strength reduction method, the safety factor and failure position of the slope can be obtained without assuming the location and form of the slip plane. And large-scale finite element software such as ABAQUS, Midas can provide convenience for the solution. Consequently, this method is widely used in engineering and is the dominating method to analyze the stability of complex rock and soil mass.

The reduction mechanism of the traditional strength reduction method is to reduce the cohesion and internal friction angle in the same proportion. By increasing the reduction coefficient, the overall safety factor can be obtained when the rock and soil reach the critical instability state [6, 7]. However, this method ignores that the cohesion and internal friction angle have a different impact on the stability of rock and soil. To make up for the defect of the traditional strength reduction method, the double strength reduction method that uses different reduction factors was proposed [8–11]. When the double strength reduction method is used to study the stability of tunnels, the uncertainty of tunnel instability modes will reduce the applicability of commonly used instability criteria. Therefore, it is necessary to focus on determining an instability criterion suitable for tunnel stability analysis. Besides, determining the appropriate reduction coefficient is the key and basis for the application of this method. There are few studies on the stability of the tunnel portal section based on the double strength reduction method at present. And most relative studies used two-dimensional models, which couldn't reflect the engineering geological conditions and the distribution characteristics of the free face. The three-dimensional model based on the strength reduction method is usually used in slope stability research [12, 13].

In this paper, based on a novel double strength reduction method (the strength reduction shortest path method), a three-dimensional model of the tunnel portal section was established to reveal the instability law of rock and soil mass. The research results of this paper could provide a reference for scientific researches and engineering application of tunnel engineering.

2 Strength Reduction Shortest Path Method

2.1 Reduction Mechanism

To obtain reasonable reduction factors, ISAKOV et al. [14] proposed a new method, namely the strength reduction shortest path method, in a study on the subgrade stability in 2010. Then they successfully applied this method to the slope stability analysis in 2014 [15]. They reduced the cohesion c and the internal friction angle φ according to different reduction factors. The reduction factor of cohesion was F_c, and the reduction factor of internal friction angle was F_φ, as shown in formula (1). The definition of the reduction factors in this method is the same as that of the double strength reduction method.

$$\begin{cases} F_c = \frac{c_0}{c_{SRT}} \\ F_\phi = \frac{tan\phi_0}{tan\phi_{SRT}} \end{cases} \tag{1}$$

Where c_0 and φ_0 are the initial cohesion and the initial internal friction angle, respectively, c_{SRT} and φ_{SRT} are the reduced cohesion and the reduced internal friction angle, respectively.

The ratio of F_c to F_φ is defined as the parameter reduction ratio λ, namely $\lambda = F_c / F_\varphi$. In Fig. 1, M_0 represents the original state of the tunnel, M_n represents a certain limit state of the tunnel (n is a positive integer). The reduction path L can be obtained by connecting M_0 and M_n, and its expression is show in formula (2).

$$L = \sqrt{\left(1 - \frac{1}{F_C}\right)^2 + \left(1 - \frac{1}{F_\varphi}\right)^2} \tag{2}$$

The reduction ratio λ theoretically has innumerable values, and correspondingly there are countless reduction paths. The limit state line is obtained by connecting all the limit state points. L_k is the traditional strength reduction path, and its intersection point with the limit state line is M_k. Among all reduction paths, there must be a reduction path that is the shortest, which is expressed as L_{min} in Fig. 1. Through this shortest reduction path (the shortest path of strength reduction), the tunnel can reach the limit state at the fastest from the initial state.

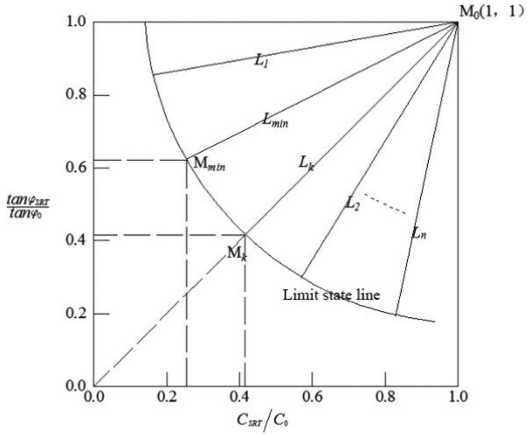

Fig. 1. Schematic diagram of the limit state line

Pan Jiazheng proposed the principle of maximum and minimum stability of rock and soil mass [16]. He believes that when the rock and soil mass become unstable, the sliding surface will provide the maximum anti-sliding force it can provide. However, this maximum anti-sliding force is the smallest of all potential sliding surfaces. Pan's principle is similar to the strength reduction shortest path method and can help us get a physical interpretation of the strength reduction method.

2.2 Definition of the Overall Safety Factor

When calculating the overall safety factor of the shear failure of the tunnel surrounding rock based on the traditional strength reduction method, because the cohesion and the

internal friction angle are reduced in the same proportion, the overall safety factor is $F_s = F_c = F_\varphi$. In this case, the overall safety factor has a clear physical meaning and can be solved simply. However, when adopting the double strength reduction method, it is difficult to calculate the overall safety factor. This is because the cohesion and the internal friction angle have different reduction factors, and their effects on the overall safety factor are difficult to evaluate quantitatively.

While ISAKOV proposed the strength reduction shortest path method, he also defined the overall safety factor (as shown in formula (3)). We adopted this overall safety factor defined by ISAKOV in this paper. By substituting formula (2) into formula (3), the final expression of overall safety factor can be obtained, as shown in formula (4).

$$F_s = \frac{1}{1 - L\Big/\sqrt{2}} \tag{3}$$

$$F_s = \frac{1}{1 - \sqrt{\left(1 - \frac{1}{F_C}\right)^2 + \left(1 - \frac{1}{F_\varphi}\right)^2}\Big/\sqrt{2}} \tag{4}$$

3 3D Model Establishment and Result Analysis

In this paper, ABAQUS was used to calculate the model. To reduce the influence of the different buried depths of the tunnel vault, we set the model upper surface to be flat. The size of the model is shown in Fig. 2. The height, the span, the buried depth of the tunnel profile is 8.18 m, 10.79 m, and 10.79 m separately. Parameters of surrounding rock in the model: bulk density $\gamma = 20\text{kN/m}^3$, initial cohesion $c_0 = 150\text{kPa}$, initial internal friction angle $\varphi_0 = 24°$, elastic modulus $E = 1.3\text{GPa}$, Poisson's ratio $\upsilon = 0.35$.

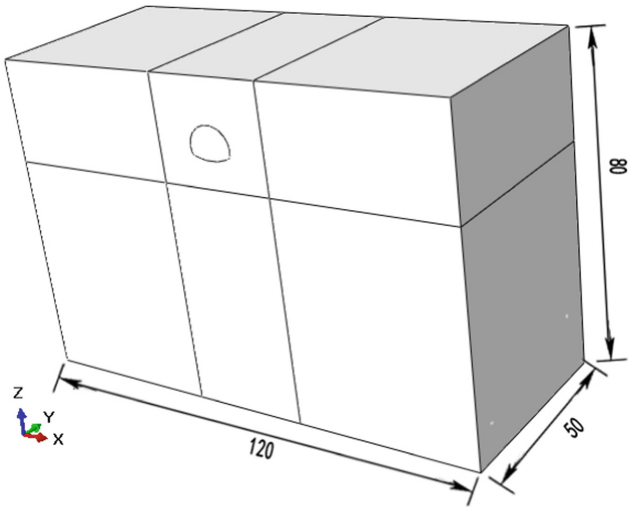

Fig. 2. Schematic diagram of the model (unit: m)

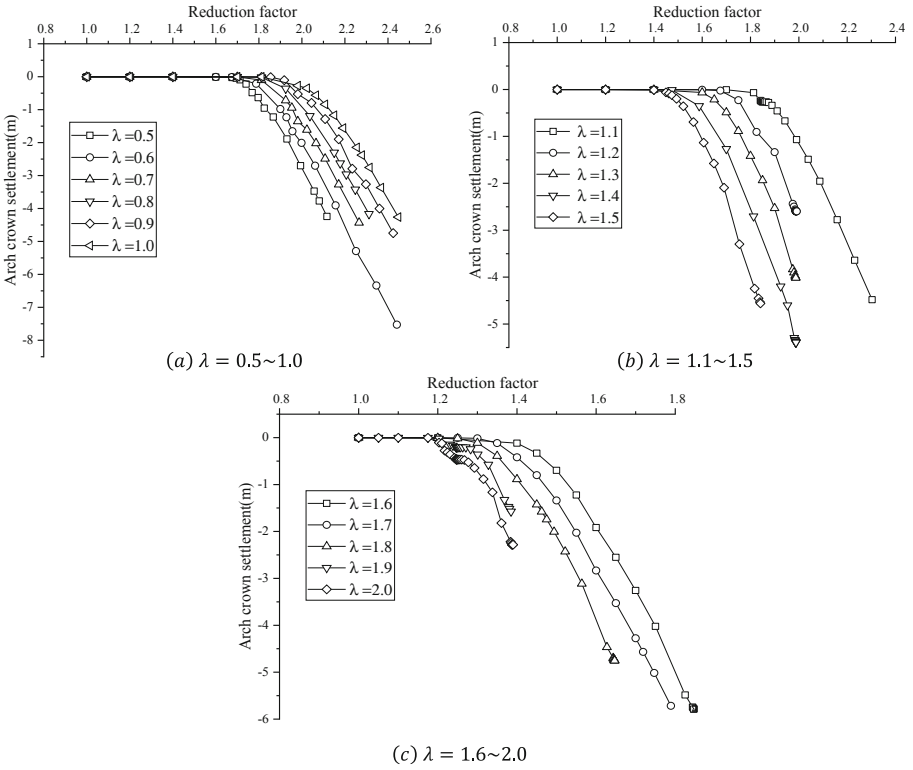

Fig. 3. Arch crown settlement curves under different reduction ratios

The arch crown settlement at the tunnel portal section under different reduction ratios is shown in Fig. 3.

By substituting the reduction factors corresponding to displacement mutation points in Fig. 3 into formula (2) and (4), we got the lengths of reduction paths and the overall safety factors under different reduction ratios separately. The calculation results are shown in Table 1.

Table 1. The overall safety factors under different reduction ratios

λ	F_c	F_φ	L^2	F_s
0.5	1.741	3.481	0.689	2.421
0.6	1.788	2.979	0.635	2.292
0.7	1.813	2.589	0.578	2.162
0.8	1.860	2.325	0.539	2.079
0.9	1.918	2.131	0.511	2.022
1.0	1.981	1.981	0.491	1.981

(*continued*)

Table 1. (*continued*)

λ	F_c	F_φ	L^2	F_s
1.1	2.025	1.841	0.465	1.931
1.2	2.100	1.750	0.458	1.918
1.3	2.145	1.650	0.440	1.884
1.4	2.223	1.588	0.440	1.882
1.5	2.241	1.494	0.416	1.838
1.6	2.240	1.400	0.388	1.787
1.7	2.295	1.350	0.386	1.783
1.8	2.340	1.300	**0.381**	**1.775**
1.9	2.414	1.271	0.389	1.788
2.0	2.534	1.267	0.411	1.829

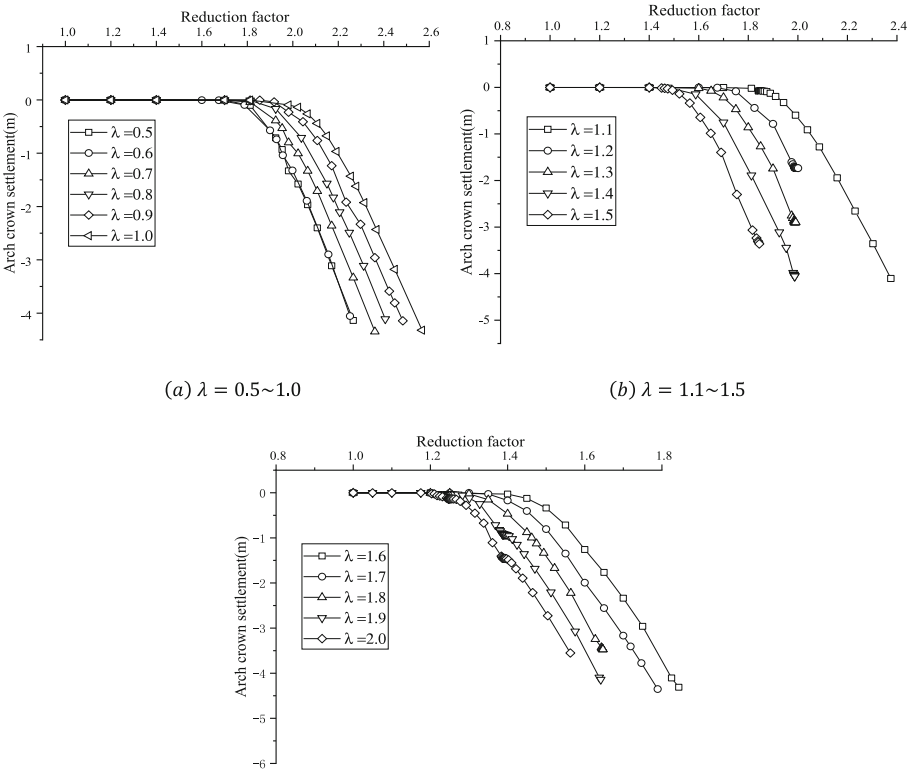

$(a)\ \lambda = 0.5{\sim}1.0$ $(b)\ \lambda = 1.1{\sim}1.5$

$(c)\ \lambda = 1.6{\sim}2.0$

Fig. 4. The arch crown settlement curve under different reduction ratios

It can be seen from Table 1 that as the reduction ratio λ increases, the reduction factor of cohesion gradually increases, while the reduction factor of internal friction angle gradually decreases. The reduction ratio λ and the overall safety factor F_s corresponding to the shortest path are 1.8 and 1.775, respectively. Research results show that the strength reduction shortest path method is suitable for the stability analysis of surrounding rock of the three-dimensional tunnel model.

The arch crown settlement of the tunnel excavation face ($Y = 50$) under different reduction ratios is shown in Fig. 4.

By substituting the reduction factors corresponding to displacement mutation points in Fig. 4 into formula (2) and (4), we got the lengths of reduction paths and the overall safety factors under different reduction ratios separately. The calculation results are shown in Table 2.

Table 2. The overall safety factors under different reduction ratios

λ	F_c	F_φ	L^2	F_s
0.5	1.813	3.625	0.725	2.514
0.6	1.900	3.167	0.693	2.430
0.7	1.925	2.750	0.636	2.293
0.8	2.038	2.547	0.628	2.275
0.9	2.045	2.272	0.574	2.155
1.0	2.108	2.108	0.552	2.108
1.1	2.137	1.943	0.518	2.037
1.2	2.190	1.825	0.500	1.999
1.3	2.275	1.750	0.498	1.996
1.4	2.310	1.650	0.477	1.954
1.5	2.346	1.564	0.459	1.920
1.6	2.400	1.500	0.451	1.905
1.7	2.465	1.450	0.450	1.901
1.8	2.520	1.400	**0.445**	**1.894**
1.9	2.600	1.369	0.451	1.905
2.0	2.676	1.338	0.456	1.914

It can be seen from Table 2 that the reduction ratio corresponding to the shortest path of the tunnel excavation face is 1.8, which is equal to that of the portal section. In both cases, the displacement mutation of the vault is taken as the instability criterion. However, the overall safety factor of the portal section is 1.894, which is greater than that of the excavation face (1.775). The above indicates that under normal circumstances, the portal section will lose stability first and is the most dangerous part of the tunnel.

In Fig. 5-a, the abscissa value represents the distance between the current section and the tunnel portal section ($Y = 0$), and the ordinate value represents the settlement of the vault. With the increase of the distance from the portal, the settlement of the tunnel

vault decreases gradually. Figure 5-b and Fig. 5-c are the settlement diagram and the plastic deformation diagram separately. The tunnel portal section is located at the red box. The number of free faces of the tunnel portal is more than that of tunnel trunk and tunnel excavation face. According to the principle of material mechanics, the more free faces a material has, the more likely it is to break. It can be seen from the figures that the portal section has the largest vault displacement, and its plastic deformation of the arch waist is the largest. Therefore, it can be concluded that the portal section ($Y = 0$) is the dangerous section of the tunnel model.

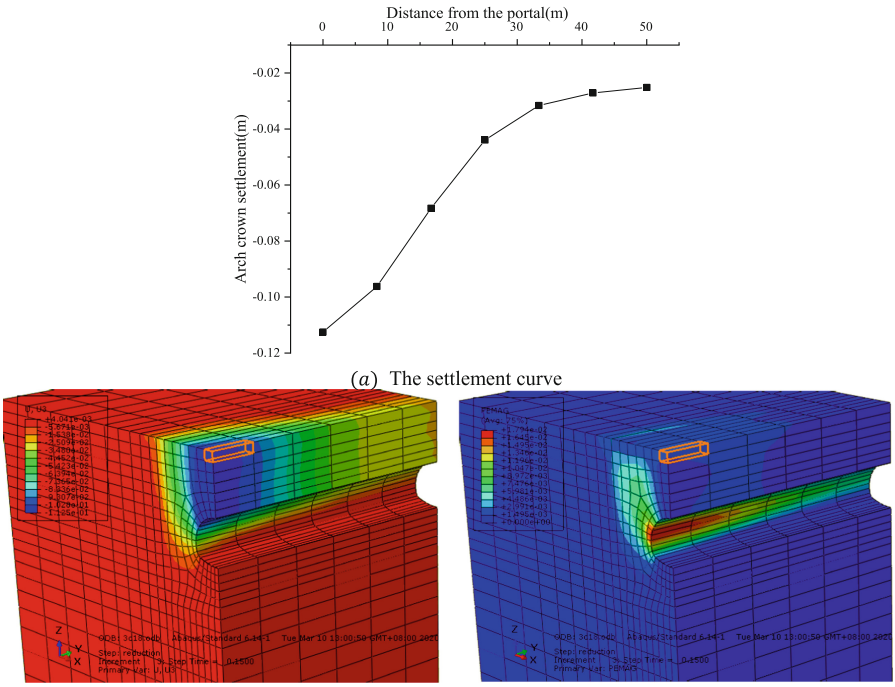

(*a*) The settlement curve

(*b*) Schematic diagram of model settlement

(*c*) Plastic deformation diagram of the model

Fig. 5. Arch crown settlement and plastic deformation at different distances from the portal section ($\lambda = 1.8$)

Figure 6 shows the distribution of surrounding rock deformation within the range of 0-50m from the tunnel portal. Because the constraint of the portal section is less than others in the tunnel, the displacement of surrounding rock in the portal is larger. And the displacement trend of vault and ground surface is subsidence. As the tunnel section moves from the portal to the tunnel excavation face, the surrounding rock displacement of the tunnel section shows a decreasing trend. The largest plastic deformation of all sections occurs at the arch waist. And the plastic deformation of the arch waist at the tunnel portal section is the greatest among all sections. With the tunnel section moving from the portal to the tunnel excavation face, the plastic deformation of the surrounding rock decreases. As the calculation time increases, the plastic deformation at the waist

expands both in the X direction and the Y direction. However, it is faster to extend in the X direction than in the Y direction. Besides, the plastic zone in the two directions gradually extends to the ground surface.

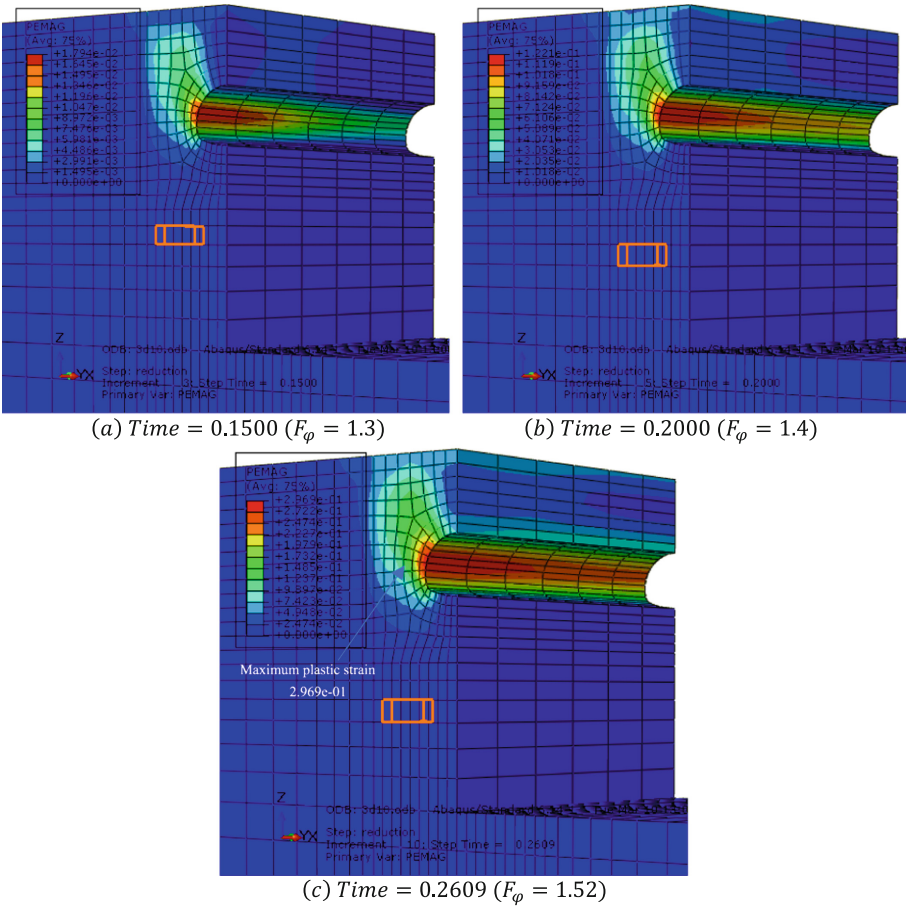

$(a)\ Time = 0.1500\ (F_\varphi = 1.3)$ $(b)\ Time = 0.2000\ (F_\varphi = 1.4)$

$(c)\ Time = 0.2609\ (F_\varphi = 1.52)$

Fig. 6. The plastic deformation diagram of the tunnel with the increase of calculation time ($\lambda = 1.8$)

The original equilibrium state of rock and soil mass at the portal is destroyed due to excavation. As a result, the rock and soil mass will have the corresponding displacement. When the vault displacement changes drastically, the tunnel vault and surrounding rock on the ground surface will collapse rapidly, which will lead to tunnel instability.

4 Influence of Strength Parameters on Stability of Surrounding Rock at the Tunnel Portal

4.1 Influence of Initial Internal Friction Angle

Four conditions of initial friction angle were set to be 20°,22°,24°, and 26°. The initial cohesion was set to be 150kPa, and the surrounding rock parameters were selected according to grade V surrounding rock. Based on the above information, the calculated data are shown in Table 3 and Table 4.

Table 3. Path lengths and overall safety factors at initial internal friction angles of 20° and 22°

$\varphi_0 = 20°$					$\varphi_0 = 22°$				
λ	F_c	F_φ	L^2	F_s	λ	F_c	F_φ	L^2	F_s
0.5	1.700	3.400	0.668	2.369	0.5	1.700	3.400	0.668	2.369
0.6	1.756	2.927	0.619	2.254	0.6	1.788	2.979	0.635	2.292
0.7	1.775	2.536	0.557	2.118	0.7	1.794	2.563	0.568	2.140
0.8	1.813	2.266	0.513	2.026	0.8	1.813	2.266	0.513	2.026
0.9	1.841	2.045	0.470	1.940	0.9	1.853	2.058	0.476	1.953
1	1.925	1.925	0.462	1.925	1	1.918	1.918	0.458	1.918
1.1	1.953	1.775	0.429	1.862	1.1	1.964	1.785	0.434	1.872
1.2	1.954	1.628	0.387	1.785	1.2	2.040	1.700	0.429	1.864
1.3	1.983	1.525	0.364	1.744	1.3	2.100	1.616	0.420	1.845
1.4	2.044	1.460	0.360	1.737	1.4	2.170	1.550	0.417	1.840
1.5	2.100	1.400	0.356	1.730	1.5	2.175	1.450	0.388	1.787
1.6	2.160	1.350	0.356	1.729	1.6	2.240	1.400	0.388	1.787
1.7	2.210	1.300	0.353	1.725	1.7	2.295	1.350	0.386	1.783
1.8	2.216	1.231	**0.336**	**1.695**	1.8	2.295	1.275	**0.365**	**1.746**
1.9	2.286	1.203	0.345	1.710	1.9	2.361	1.243	0.370	1.755
2	2.375	1.187	0.360	1.737	2	2.416	1.208	0.373	1.760

As can be seen from Table 3 and Table 4, the reduction ratio (corresponding to the shortest path of strength reduction) is the same for the four conditions with different initial internal friction angles, all of which are 1.8. The shortest path length (L_{min}) and the overall safety factor (F_s) corresponding to the four conditions all increase with the increase of initial internal friction angle (φ_0). When λ is 1.8, the vault settlement under four initial internal friction angle conditions is shown in Fig. 7. When the reduction factor is the same, the higher the initial internal friction angle is, the smaller the settlement of the arch crown is. When the displacement changes drastically, the reduction factor increases with the increase of the initial internal friction angle (φ_0).

Table 4. Path lengths and safety factors at initial internal friction angles of 24° and 26°

$\varphi_0 = 24°$					$\varphi_0 = 26°$				
λ	F_c	λ	F_c	λ	F_c	λ	F_c	λ	F_c
0.5	1.741	3.481	0.689	2.421	0.5	1.700	3.400	0.668	2.369
0.6	1.788	2.979	0.635	2.292	0.6	1.775	2.958	0.629	2.277
0.7	1.813	2.589	0.578	2.162	0.7	1.813	2.589	0.578	2.162
0.8	1.860	2.325	0.539	2.079	0.8	1.918	2.397	0.569	2.143
0.9	1.918	2.131	0.511	2.022	0.9	1.981	2.201	0.543	2.088
1	1.981	1.981	0.491	1.981	1	1.981	1.981	0.491	1.981
1.1	2.025	1.841	0.465	1.931	1.1	2.063	1.875	0.483	1.967
1.2	2.100	1.750	0.458	1.918	1.2	2.130	1.775	0.472	1.945
1.3	2.145	1.650	0.440	1.884	1.3	2.210	1.700	0.469	1.940
1.4	2.223	1.588	0.440	1.882	1.4	2.240	1.600	0.447	1.897
1.5	2.241	1.494	0.416	1.838	1.5	2.285	1.523	0.434	1.872
1.6	2.240	1.400	0.388	1.787	1.6	2.340	1.463	0.428	1.861
1.7	2.295	1.350	0.386	1.783	1.7	2.345	1.380	0.405	1.818
1.8	2.340	1.300	**0.381**	**1.775**	1.8	2.340	1.300	**0.381**	**1.775**
1.9	2.414	1.271	0.389	1.788	1.9	2.428	1.278	0.393	1.797
2	2.534	1.267	0.411	1.829	2	2.525	1.263	0.408	1.824

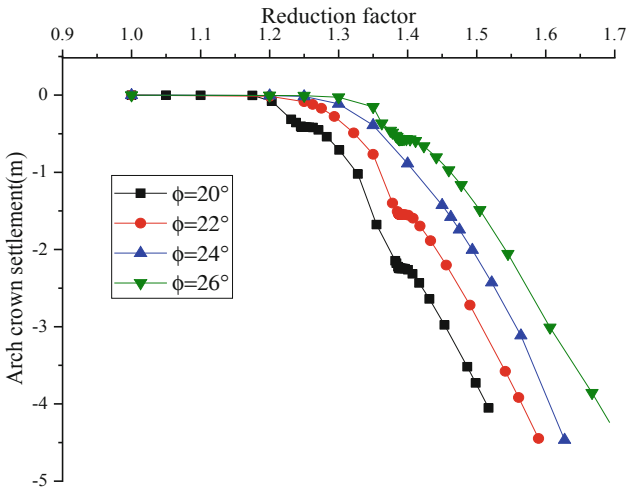

Fig. 7. Comparison of tunnel vault settlement under different initial internal friction angles (λ = 1.8)

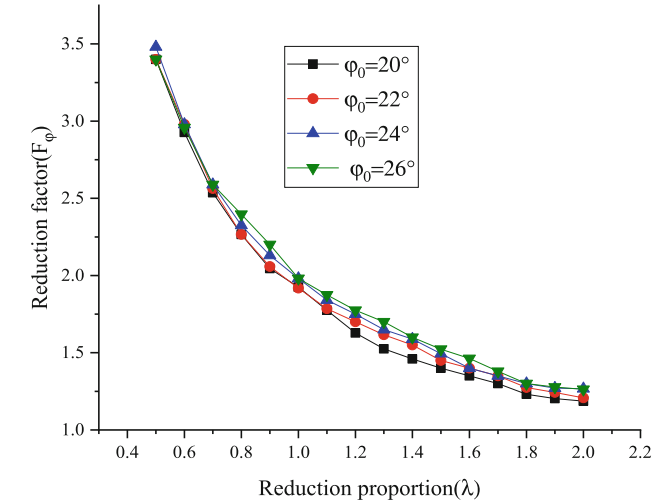

(a) The internal friction angle reduction factor F_φ

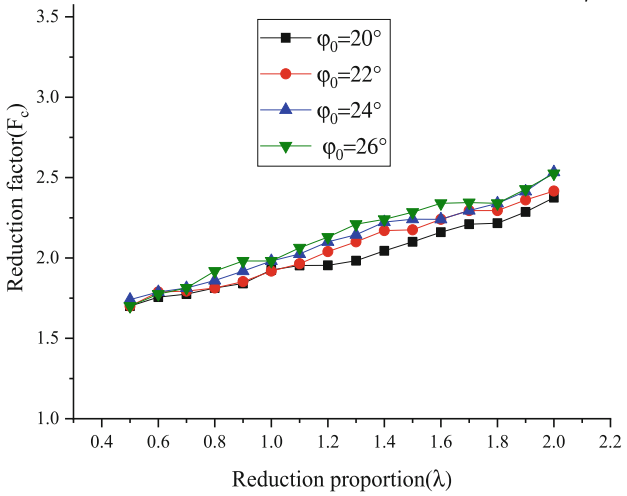

(b) The cohesion reduction factor F_c

Fig. 8. Reduction curves under different initial internal friction angles

It can be seen from Table 3, Table 4, and Fig. 8 that under the limit state, with the increase of initial internal friction angle, both the reduction factor of internal friction angle and the reduction factor of cohesion increase, but the growth rate of both gradually slows down. Therefore, in the actual project, when strengthening the surrounding rock, it is unreasonable to increase the internal friction angle blindly. Because when the internal friction angle exceeds a certain value, the improvement measures are neither economic nor ideal.

With the increase of the initial internal friction angle, although the reduction factor under the limit state increases, the growth rate of the reduction factor under different

reduction proportions is not equal. The internal friction angle reduction factor in the range of $\lambda = 1.0 - 1.8$ in Fig. 8-a and cohesion reduction factor in the range of $\lambda = 1.2 - 2.0$ in Fig. 8-b are extracted, as shown in Fig. 9.

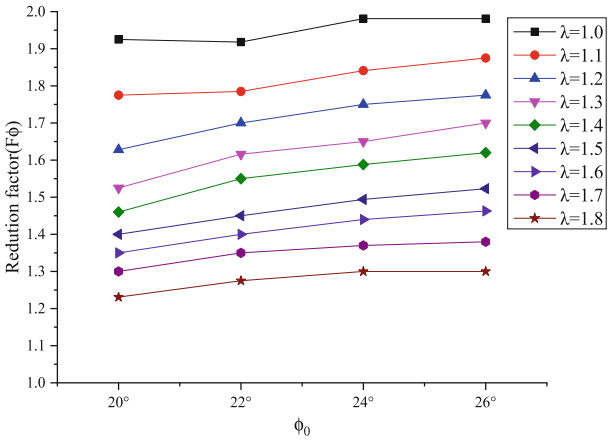

(a) The internal friction angle reduction factor F_{φ} $(\lambda = 1.0 - 1.8)$

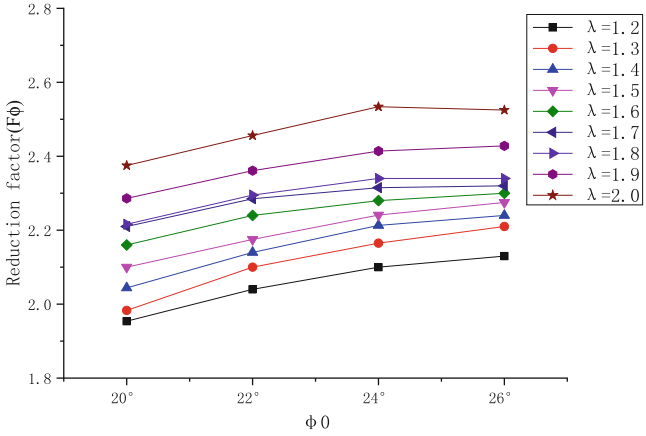

(b) The cohesion reduction factor F_c ($\lambda = 1.2 - 2.0$)

Fig. 9. Diagram of reduction factors under different reduction proportions

From Fig. 9-a, when the reduction ratio λ is in the range of 1.0–1.4, with the increase of the initial internal friction angle, the increase rate of the reduction factor F_{φ} is greater. That is, the internal friction angle in this range has a greater contribution to the resistance of the surrounding rock to deformation. From Fig. 9-b, when the reduction ratio λ is in the range of 1.4–1.6, with the increase of the initial internal friction angle, the increase rate of reduction coefficient F_c is greater. That is, the cohesion in this range contributes more to the resistance of the surrounding rock deformation.

The essence of the double strength reduction method can explain the above phenomenon. The essence of the double strength reduction method is to obtain the reduction factor of cohesion and the reduction factor of the internal friction angle separately (the two factors are not equal). Then the strength parameters of the rock and soil mass are reduced according to the determined reduction factors so that the rock and soil mass reaches the limit state from the initial state. In the reduction process, because of the different initial setting conditions (different reduction ratios), the coordination between strength parameters is complex. The analysis in this paper well reflects this essence. However, more research is needed on the influence of the reduction law of double strength parameters on the stability of surrounding rock.

Figure 10 shows the comparison of tunnel plastic deformation under different initial internal friction angles. It can be seen from the figure that with the increase of the initial internal friction angle, the failure form of the surrounding rock remains unchanged when the vault displacement changes drastically, and the plastic deformation shows a decreasing trend.

Figure 11 shows the comparison of tunnel settlement displacement under different initial internal friction angles. It can be seen from the figure that with the increase of the initial internal friction angle, the failure form of the surrounding rock remains unchanged when the vault displacement changes drastically, and the settlement shows a decreasing trend.

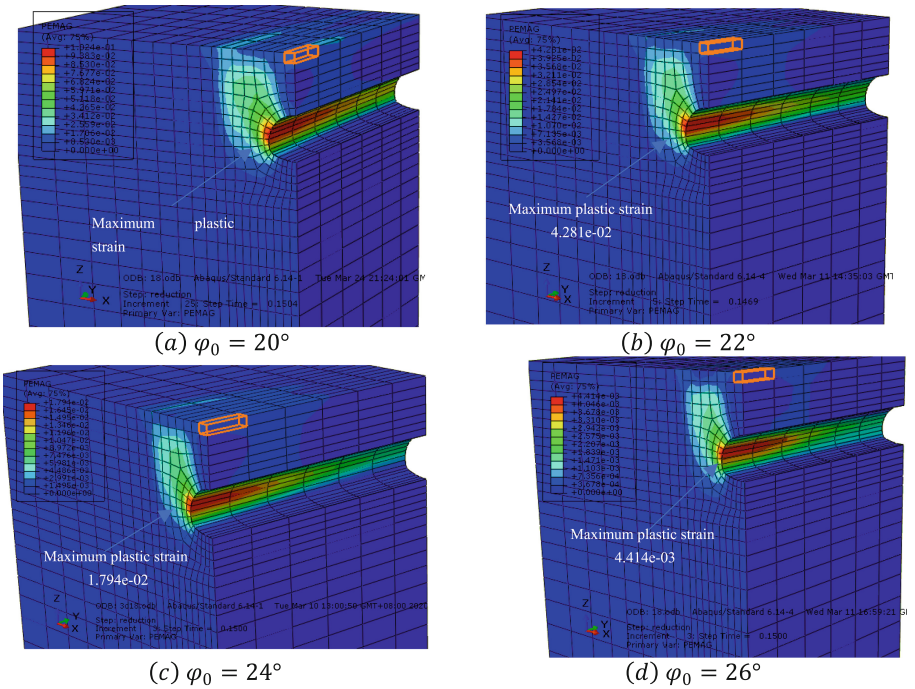

$(a)\ \varphi_0 = 20°$ $(b)\ \varphi_0 = 22°$

$(c)\ \varphi_0 = 24°$ $(d)\ \varphi_0 = 26°$

Fig. 10. The plastic deformation of the tunnel under different initial internal friction angles

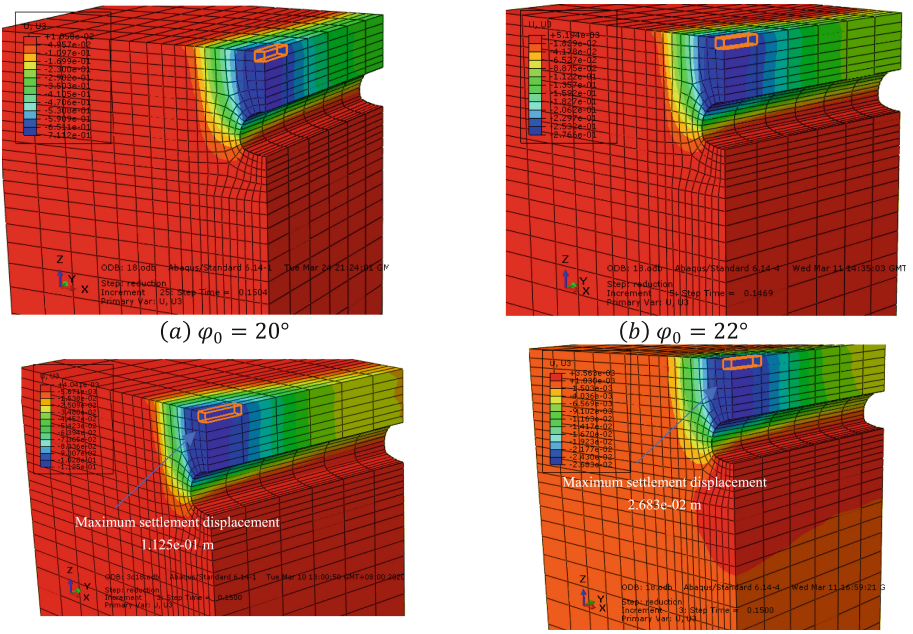

$(a)\ \varphi_0 = 20°$ $(b)\ \varphi_0 = 22°$

$(c)\ \varphi_0 = 24°$ $(d)\ \varphi_0 = 26°$

Fig. 11. Tunnel settlement displacement diagram under different initial internal friction angles

4.2 Influence of Initial Cohesion

Three conditions of initial cohesion were set to be 100 kPa, 150 kPa, and 200 kPa. The initial friction angle was set to be 24°, and the surrounding rock parameters were selected according to grade V surrounding rock. Based on the above information, the calculated data is shown in Table 5.

It can be seen from Table 3 that with the increase of initial cohesion c_0, the reduction ratio λ corresponding to the shortest path L_{min} increases. With the increase of initial cohesion c_0, both the shortest path length and safety factor show an increasing trend. The square of reduction path length L^2 and reduction ratio λ corresponding to different initial cohesion c_0 in Table 3 were extracted, and the extracted data were parabola fitted, as shown in Fig. 12.

In Fig. 12, the positions of the three parabolas gradually move up with the increase of the cohesion, which proves that the path length shows an increasing trend; The symmetry axis of the parabola also gradually moves to the right with the increase of the cohesion, that is, the reduction proportion corresponding to the shortest path increases.

It can be seen from Table 5 and Fig. 13 that under the limit state, with the increase of the initial cohesion, both the reduction factor of internal friction angle and the reduction factor of cohesion show an increasing trend. But the growth rate of the two will show a downward trend, which is consistent with the law under different initial internal friction angle conditions. Therefore, in the actual project, when strengthening the surrounding rock, it is unreasonable to increase the cohesion blindly. Because when the value of the cohesion exceeds a certain value, the improvement measures are neither economic nor ideal. With the increase of initial cohesion, although the reduction factor in the limit

Table 5. Path lengths and safety factors corresponding to different initial cohesions

	$c_0 = 100KPa$				$c_0 = 150KPa$				$c_0 = 200KPa$			
λ	F_c	F_φ	L^2	F_s	F_c	F_φ	L^2	F_s	F_c	F_φ	L^2	F_s
0.5	1.250	2.500	0.400	1.809	1.741	3.481	0.689	2.421	2.150	4.300	0.875	2.954
0.6	1.300	2.167	0.343	1.707	1.788	2.979	0.635	2.292	2.263	3.771	0.851	2.877
0.7	1.400	2.000	0.332	1.687	1.813	2.589	0.578	2.162	2.319	3.313	0.811	2.753
0.8	1.450	1.813	0.297	1.627	1.860	2.325	0.539	2.079	2.361	2.951	0.769	2.633
0.9	1.438	1.597	0.232	1.517	1.918	2.131	0.511	2.022	2.488	2.764	0.765	2.621
1	1.475	1.475	0.207	1.475	1.981	1.981	0.491	1.981	2.572	2.572	0.747	2.572
1.1	1.54	1.4	0.205	1.470	2.025	1.841	0.465	1.931	2.613	2.375	0.716	2.490
1.2	1.596	1.33	0.201	1.464	2.100	1.750	0.458	1.918	2.580	2.150	0.661	2.353
1.3	1.641	1.263	0.196	1.456	2.145	1.650	0.440	1.884	2.576	1.981	0.620	2.255
1.4	1.678	1.198	**0.191**	**1.447**	2.223	1.588	0.440	1.882	2.695	1.925	0.626	2.271
1.5	1.752	1.168	0.205	1.471	2.241	1.494	0.416	1.838	2.719	1.813	0.601	2.212
1.6	1.846	1.154	0.228	1.510	2.240	1.400	0.388	1.787	2.780	1.738	0.590	2.189
1.7	1.96	1.153	0.258	1.560	2.295	1.350	0.386	1.783	2.890	1.700	0.597	2.205
1.8	2.064	1.147	0.282	1.602	2.340	1.300	**0.381**	**1.775**	2.970	1.650	0.595	2.200
1.9	2.159	1.136	0.303	1.637	2.414	1.271	0.389	1.788	2.898	1.525	**0.547**	**2.097**
2	2.27	1.135	0.327	1.679	2.534	1.267	0.411	1.829	2.988	1.494	0.552	2.107

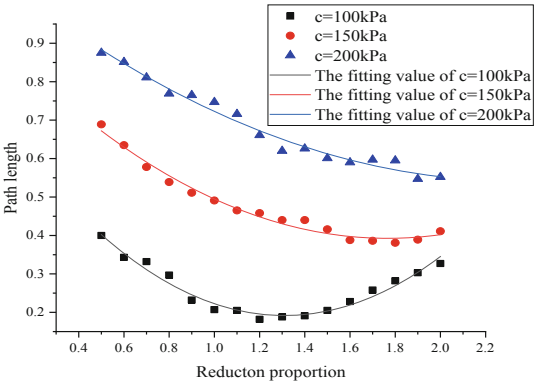

Fig. 12. Path lengths at different reduction proportions

state increases, the growth rate of the reduction factor in different reduction proportion ranges is not equal. Extract the reduction factor data of Fig. 13, as shown in Fig. 14.

From Fig. 14-a, when the reduction ratio λ is in the range of 0.5–1.1, with the increase of the initial cohesion, the increase rate of the reduction factor F_φ is greater. That is, the initial cohesion in this range has a greater contribution to the resistance of surrounding rock to deformation. From Fig. 14-b, when the reduction ratio λ is in the range of 0.5–2.0, with the increase of the initial cohesion, the growth rate of the reduction factor F_c

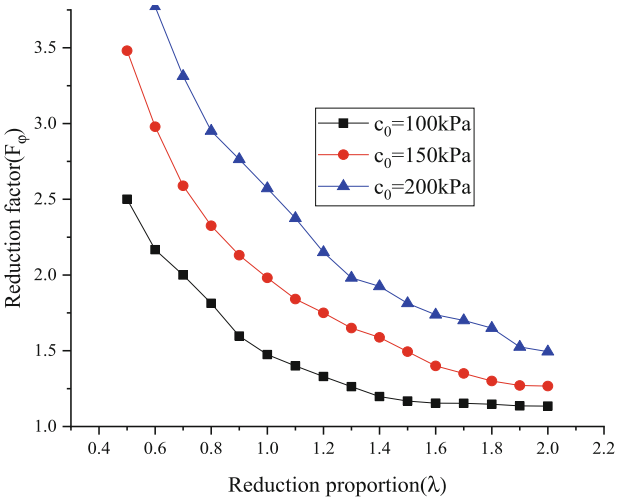

(a) The internal friction angle reduction factor F_φ

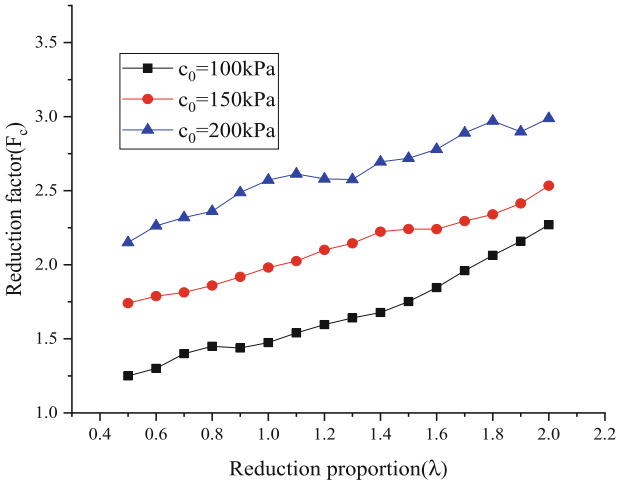

(b) The cohesion reduction factor F_c

Fig. 13. Reduction curve under different initial cohesions

is nearly unchanged. That is, the reduction ratio λ will not have a significant impact on the increase of the reduction factor of cohesion.

Figures 15 and 16 show the tunnel plastic deformation and tunnel settlement displacement under different initial cohesions respectively. It can be seen from the figures that with the increase of the initial cohesion, the failure form of the tunnel surrounding rock remains unchanged when the vault displacement changes drastically, and the settlement shows a decreasing trend.

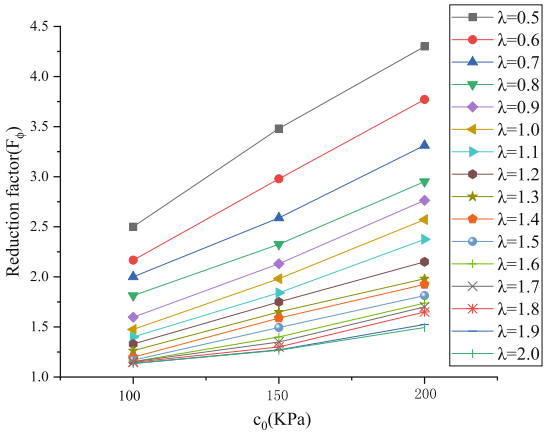

(a) The internal friction angle reduction factor F_φ $(\lambda = 1.0 - 1.8)$

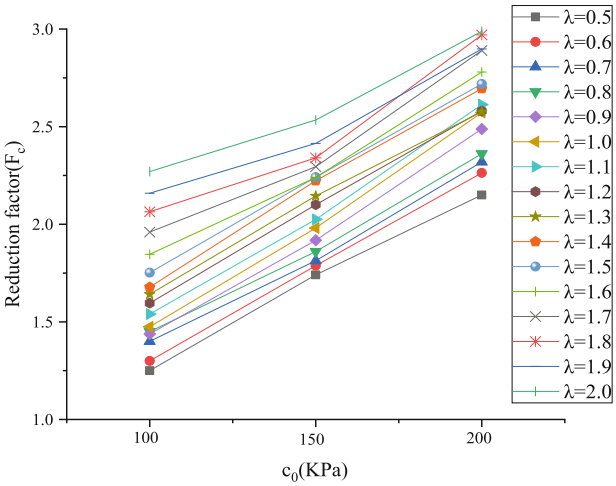

(b) The cohesion reduction factor F_c $(\lambda = 1.2 - 2.0)$

Fig. 14. Variation chart of reduction factors under different reduction ratios

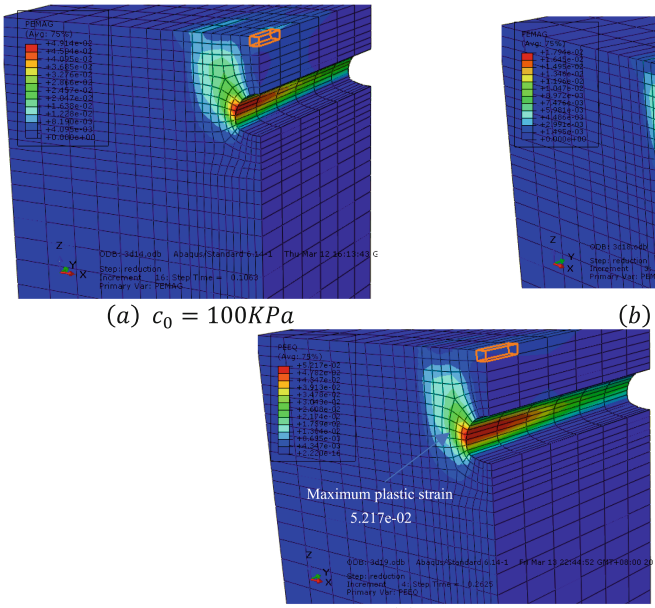

$(a)\ c_0 = 100KPa$ $(b)\ c_0 = 150KPa$

$(c)\ c_0 = 200KPa$

Fig. 15. Tunnel plastic deformation under different initial cohesions

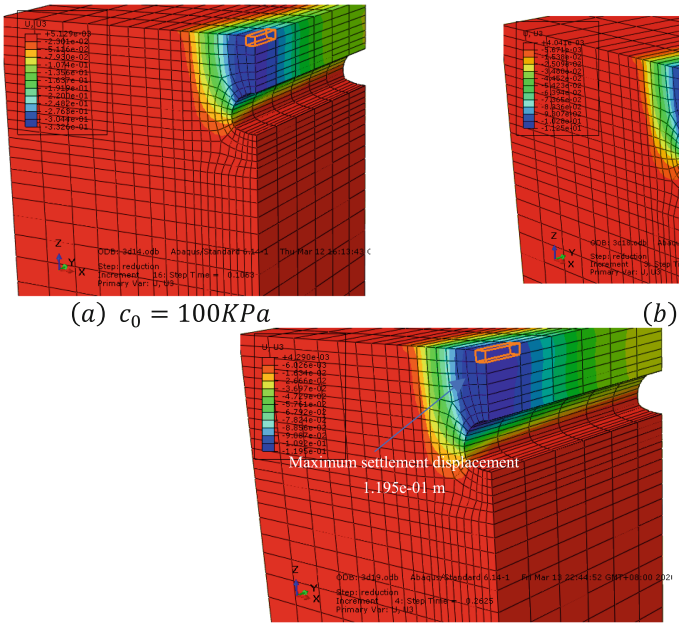

$(a)\ c_0 = 100KPa$ $(b)\ c_0 = 150KPa$

$(c)\ c_0 = 200KPa$

Fig. 16. Tunnel settlement displacement diagram under different initial cohesions

5 Conclusion

In this paper, a three-dimensional model of the tunnel portal section was established and analyzed. The stability analysis results of the surrounding rock at the tunnel portal verified the applicability of the strength reduction shortest path method to the three-dimensional model. Besides, the stability of tunnel surrounding rock with different strength parameters was studied by a numerical method, and the changing rules of the surrounding rock failure form were analyzed. The main conclusions are as follows.

1) As the reduction ratio λ increases, the length of the strength reduction path decreases first and then increases. And the variation conforms to the parabolic characteristics, indicating that there is the shortest path for the strength reduction. Thence the applicability of the strength reduction shortest path method in the finite element analysis of the three-dimensional tunnel model is verified.
2) It is reasonable to select the tunnel portal section as the most dangerous section in the three-dimensional model with a flat ground surface.
3) By comparing and analyzing the influence of strength parameters on the reduction factors, it was found that under the limit state, with the increase of strength parameters, both the reduction factor of internal friction angle and the reduction factor of cohesion increase. But their growth rate both shows a downward trend. Therefore, in the actual project, when strengthening the surrounding rock, it is unreasonable to increase strength parameters blindly. Because when the strength parameters exceed a certain value, the improvement measures are neither economic nor ideal.
4) Through the comparative analysis of the influence of strength parameters on the plastic deformation and settlement of the tunnel portal section, we found that the stability of the tunnel portal section increases with the increase of the strength parameters. But the change of the strength parameters has no significant effect on the failure mode of the tunnel portal section. In practical engineering, the reinforcement of the surrounding rock of the tunnel portal section can enhance the overall stability of the tunnel. But reinforcement measures can't change the distribution of dangerous parts. Therefore, continuous accident prevention should be carried out at the tunnel portal section.
5) The simulation in this study is based on the theoretical model and can predict the trend of soil deformation in case of tunnel failure. However, there may be some deviations from the actual tunnel conditions, and actual engineering simulations will be the next direction of research.

Acknowledgements. Project (2018JJ2519) supported by Hunan Provincial Natural Science Foundation of China.

References

1. Perazzelli, P., Leone, T., Anagnostou, G.: Tunnel face stability under seepage flow conditions. Tunn. Undergr. Space Technol. **43**, 459–469 (2014)

2. Anagnostou, G., Perazzelli, P.: Analysis method and design charts for bolt reinforcement of the tunnel face in cohesive-frictional soils. Tunn. Undergr. Space Technol. **47**, 162–181 (2015)
3. Lee, I.M., Lee, J.S., Nam, S.W.: Effect of seepage force on tunnel face stability reinforced with multi-step pipe grouting. Tunn. Undergr. Space Technol. **19**(6), 551–565 (2004)
4. Pan, Q., Dias, D.: Upper-bound analysis on the face stability of a non-circular tunnel. Tunn. Undergr. Space Technol. **62**, 96–102 (2017)
5. Griffiths, D.V., Lane, P.A.: Slope stability analysis by finite elements. Geotechnique **49**(3), 387–403 (1999)
6. Lian, Z., Han, G., Kong, X.: Stability analysis of excavation by strength reduction FEM. Chinese J. Geot. Eng. **23**(4), 407–411 (2001)
7. Zhang, P., Chen, Z.: Influences of soil elastic modulus and Poisson's ratio on slope stability. Rock Soil Mech. **27**(2), 299–303 (2006)
8. Tang, F., Zheng, Y.: Mechanism analysis on dual reduction factors about the progressive failure of slope. Chin. J. Undergr. Space Eng. **4**(3), 436–441+464 (2008)
9. Tang, F., Zheng, Y.: Analysis on safety reserve of slope with two strength reduction factor. J. Chongqing Jiaotong Univ. (Nat. Sci.) **26**(4), 95–100 (2007)
10. Tang, F., Zheng, Y.: Mechanism analysis on dual reduction factors about the progressive failure of slope. Chin. J. Undergr. Space Eng. **4**(3), 436–441+464 (2008)
11. Tang, F., Zheng, Y.: Effect on safety factors in different definitions based on strength margin. J. Civil Arch. Environ. Eng. **31**(3), 61–65+97 (2009)
12. Zheng, Y., Zhao, S., Song, Y.: Advance of study on the strength reduction finite element method. J. Logist. Eng. Univ. (03), 1–6 (2005)
13. Zhang, K.: Three-dimensional slope stability and failure analysis using shear strength reduction finite element method (SSR-FEM). Dalian University of Technology (2011)
14. Isakov, A., Korneyev, D.A., Moryachkov, Y.: Two-parameter criterion of road bed stability. In: Proceedings of Engineering Geology, Soil Mechanics and Foundations. Novosibirsk, Russia: [s. n.], pp. 31–38 (2010)
15. Isakov, A., Moryachkov, Y.: Estimation of slope stability using two-parameter criterion of stability. Int. J. Geomech. **14**(3), 613–624 (2014)
16. Chen, Z.: On Pan's principles of soil and rock stability analysis. J. Tsinghua Univ. Sci. Technol. **38**(1), 3–6 (1998)